

Inverse Design and Control of Microstructural Development in Solidification Processes with Natural Convection

George Z. Yang and Nicholas Zabaras

Sibley School of Mechanical and Aerospace Engineering
188 Frank H. T. Rhodes Hall, Cornell University
Ithaca, NY 14853-3801

ABSTRACT

This paper presents a finite element solution of an inverse solidification design problem. It is based on our previous work on an adjoint method with a functional optimization scheme for the solution of inverse thermal convection problems with overspecified thermal boundary conditions. An inverse calculation is performed here for directional solidification processes to find the optimal heat flux at the mold wall boundary on both the solid and liquid mold sides. The objective is to achieve desired velocity and heat flux histories at the solid-liquid interface. The specification of the growth velocity and freezing interface heat fluxes considers the microstructural implications on the casting product and the morphological stability requirements of the freezing interface. An example of solidification in a rectangular mold with a planar interface growth is shown.

NOMENCLATURE

English:

c_l liquid specific heat
 C_o liquid concentration
 D_l liquid solute diffusivity
 e_g unit vector in the direction of gravity
 G temperature gradient
 I unit second order tensor
 k solid-liquid equilibrium partition ratio
 l length scale
 L latent heat of solidification
 L_2 Lebesgue square integrable functional space
 m_l slope of the liquidus in a binary phase diagram
 n normal out of boundary of the liquid domain
 p dimensionless pressure
 Pr Prandtl number
 q dimensionless heat flux
 Ra Rayleigh number = $\frac{g\beta(T_i - T_m)l^3}{\alpha\nu}$
 s dimensionless position of the solid-liquid interface
 S objective function for inverse optimization
 Ste Stefan number (ratio of sensible to latent heat)

t dimensionless time
 T temperature
 T_m melting (freezing) temperature
 T_i reference or initial (uniform) liquid temperature
 u dimensionless velocity vector
 v velocity vector
 v_f solid-liquid interface velocity
 U sensitivity velocity vector
 x dimensionless spatial coordinates in the domain Ω

Greek:

α thermal diffusivity
 β thermal expansion coefficient
 Γ boundary of the domain Ω
 θ dimensionless temperature
 Θ dimensionless sensitivity temperature
 ν kinematic viscosity
 Π dimensionless sensitivity pressure
 σ dimensionless stress tensor
 Σ dimensionless sensitivity stress tensor
 π dimensionless adjoint pressure
 ζ dimensionless adjoint stress tensor
 ϕ dimensionless adjoint velocity
 ψ dimensionless stream function
 Ψ dimensionless adjoint temperature

Subscripts:

g essential boundary condition
 h natural boundary condition
 I at the solid-liquid interface
 l liquid
 o for unknown flux at the solid or liquid boundary
 s solid

INTRODUCTION

Solidification phenomena have extensive industrial applications including metal casting and crystal growth processes [1-2]. Heat transfer and fluid flow play essential roles in these processes [2]. Inverse design of solidi-

fication processes through thermal boundary condition design has been investigated in a number of cases [3-6].

Here, we are interested in the design of solidification processes with thermal convection in the liquid melt. The formulation involves the temporal and spatial temperature and velocity fields. It can be applied to solidification of pure substances or to dilute alloy solidification with a sharp solid-liquid interface. For the latter case, a simplification will be made by neglecting the inhomogeneity of solute concentration.

The inverse design is realized with a proper selection of the heat flux q_o on the mold boundary Γ_o that leads to a desired flux q_l on the freezing interface and a desired growth velocity v_f . The inverse problems in the solid and liquid regions are fully uncoupled.

Our formulation is based on a functional optimization scheme which was developed earlier by the authors for the analysis of inverse natural convection problems in fixed enclosures [7]. In particular, reference [7] presented an algorithm for the calculation of the heat flux in part of the boundary of a convecting fluid using overspecified thermal boundary conditions (heat flux and temperature) at another part of the boundary. The developed inverse technique uses the adjoint method to calculate in the L_2 space the derivative of the cost functional $\|T(\mathbf{x}_I, t; q_o) - T_m\|_{L_2}^2$ which is the square error between the calculated temperature at the freezing interface Γ_I and the given melting temperature. The minimization of the cost functional was performed by the conjugate gradient method via the solution of the direct, adjoint and sensitivity problems. The inverse problem in the solid region is an inverse heat conduction problem [8] on a deforming domain. It has been studied earlier [3-6] and here emphasis will only be given to the inverse problem in the melt where the calculation of the gradient of the cost functional requires a proper coupling between the thermal and fluid flow operators of the adjoint problem.

The capability of control of the temporal growth velocity v_f and heat flux q_{ll} at the interface liquid side, enables the control of the microstructure development during solidification [1-2]. We prefer to choose spatially uniform q_{ll} and v_f that result in uniform microstructure. Dendritic morphology or mushy layer is to be avoided which means that the stability of sharp solid-liquid interface is to be maintained. Stability criteria are well established [2, 9-10] to relate q_{ll} and v_f . Here, we choose to estimate and satisfy such criteria with a simplified form [10]:

$$\left| \frac{G_{ll}}{v_f} \right| \geq \frac{|m_l|(1-k)C_o}{D_l} \quad (1)$$

The basic physics for this criteria is to avoid constitutional supercooling [2], although in our case, the concentration field is not calculated.

INVERSE FORMULATION

We present the formulation of the inverse problem in the liquid region only.

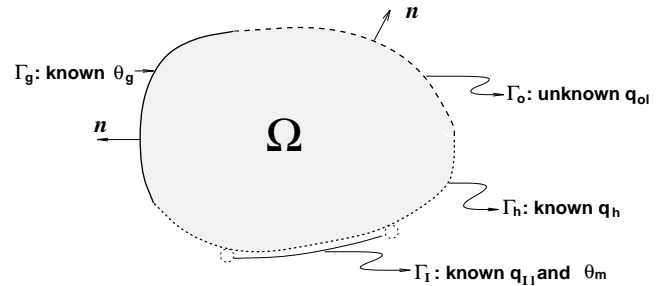


FIGURE 1: Schematic of the inverse problem in the melt.

Let us consider the domain Ω which is occupied by the solidifying liquid melt. The liquid melt is assumed to have temperature-independent thermal physical properties. The melt flow is driven by a *Boussinesq* buoyancy effect and we only consider such a natural convection in the laminar flow regime. We are interested in the spatial and temporal temperature $T(\mathbf{x}, t)$ and velocity $\mathbf{v}(\mathbf{x}, t)$ fields. Γ is the boundary of Ω . According to the type of thermal boundary condition, Γ is divided into: the solid-liquid interface Γ_I that is at the melting temperature T_m , the essential boundary Γ_g where temperature is known, the natural boundary Γ_h where heat flux is known, and Γ_o which is the boundary with *unknown flux* q_{ol} . These boundaries are shown in Figure 1. In the rest of this paper the notation will be in non-dimensional form. The dimensionless temperature is defined as $\theta = \frac{T - T_m}{T_i - T_m}$, and the dimensionless velocity by $\mathbf{u} = \frac{\mathbf{v}l}{\alpha}$, where we have taken l as length scale and l^2/α as the time scale. The governing equations are:

$$\frac{\partial \theta}{\partial t} + \mathbf{u} \cdot \nabla \theta = \nabla \cdot \nabla \theta \quad (2)$$

$$\frac{\partial \mathbf{u}}{\partial t} + \mathbf{u} \cdot \nabla \mathbf{u} = \nabla \cdot \boldsymbol{\sigma} - RaPr\theta \mathbf{e}_g \quad (3)$$

$$\boldsymbol{\sigma} = -p\mathbf{I} + Pr[\nabla \mathbf{u} + (\nabla \mathbf{u})^T] \quad (4)$$

$$\nabla \cdot \mathbf{u} = 0 \quad (5)$$

$$\theta(\mathbf{x}, 0) = \theta_i(\mathbf{x}), \quad \mathbf{x} \in \Omega \quad (6)$$

$$\mathbf{u}(\mathbf{x}, 0) = 0, \quad \mathbf{x} \in \Omega \quad (7)$$

$$\mathbf{u}(\mathbf{x}, t) = 0, \quad (\mathbf{x}, t) \in \Gamma \times [0, t_{max}] \quad (8)$$

$$\theta(\mathbf{x}, t) = \theta_g, \quad (\mathbf{x}, t) \in \Gamma_g \times [0, t_{max}] \quad (9)$$

$$\frac{\partial \theta}{\partial n}(\mathbf{x}, t) = q_h(\mathbf{x}, t), \quad (\mathbf{x}, t) \in \Gamma_h \times [0, t_{max}] \quad (10)$$

$$\frac{\partial \theta}{\partial n}(\mathbf{x}, t) = q_{ll}(\mathbf{x}, t), \quad (\mathbf{x}, t) \in \Gamma_I \times [0, t_{max}] \quad (11)$$

$$\frac{\partial \theta}{\partial n}(\mathbf{x}, t) = q_{ol}(\mathbf{x}, t), \quad (\mathbf{x}, t) \in \Gamma_o \times [0, t_{max}] \quad (12)$$

The equations above define a well posed *direct problem* for each heat flux q_{ol} on Γ_o , with the temporal position of Γ_I assumed to be known. Note that the temperature condition, $\theta = \theta_m = 0$, at Γ_I , is not part of the definition of the above direct problem. Instead, it can be used to define an optimization problem for the calculation of the flux q_{ol} . For a guess q_{ol} , we can define a discrepancy at Γ_I between the calculated temperature from the above direct problem, $\theta(\mathbf{x}, t; q_{ol})$, and the given melting temperature, $\theta_m = 0$. The following cost functional can then be defined:

$$\begin{aligned} S(q_{ol}) &= \frac{1}{2} \|\theta(\mathbf{x}, t)\|_{L_2(\Gamma_I \times [0, t_{max}])}^2 \\ &= \frac{1}{2} \int_0^{t_{max}} \int_{\Gamma_I} \theta(\mathbf{x}, t)^2 d\Gamma dt \end{aligned} \quad (13)$$

The solution process for the calculation of the optimal q_{ol} leads to the minimization of $S(q_{ol})$. It can be shown [7] that the derivative $S'(q_{ol})$ of the cost functional in the $L_2(\Gamma_I \times [0, t_{max}])$ space is:

$$S'(q_{ol}(\mathbf{x}, t)) = \Psi(\mathbf{x}, t), \quad (\mathbf{x}, t) \in \Gamma_o \times [0, t_{max}] \quad (14)$$

The *adjoint temperature* field $\Psi(\mathbf{x}, t)$ is coupled with the *adjoint velocity* field $\phi(\mathbf{x}, t)$. They are defined from the following *adjoint problem*:

$$\frac{\partial \Psi}{\partial t} + \mathbf{u} \cdot \nabla \Psi = -\nabla^2 \Psi + \phi \cdot \mathbf{e}_g \quad (15)$$

$$\begin{aligned} \frac{\partial \phi}{\partial t} + \mathbf{u} \cdot \nabla \phi - (\nabla \mathbf{u})^T \phi &= -\nabla \cdot \zeta + PrRa\Psi\nabla\theta \\ & \quad (16) \end{aligned}$$

$$\zeta(\mathbf{x}, t) = -\pi \mathbf{I} + Pr[\nabla \phi + (\nabla \phi)^T] \quad (17)$$

$$\nabla \cdot \phi = 0 \quad (18)$$

$$\Psi(\mathbf{x}, t_{max}) = 0, \quad \mathbf{x} \in \Omega \quad (19)$$

$$\phi(\mathbf{x}, t_{max}) = 0, \quad \mathbf{x} \in \Omega \quad (20)$$

$$\phi(\mathbf{x}, t) = 0, \quad (\mathbf{x}, t) \in \Gamma \times [0, t_{max}] \quad (21)$$

$$\Psi(\mathbf{x}, t) = 0, \quad (\mathbf{x}, t) \in \Gamma_g \times [0, t_{max}] \quad (22)$$

$$\begin{aligned} \frac{\partial \Psi}{\partial n} &= 0, \quad (\mathbf{x}, t) \in (\Gamma_h + \Gamma_o) \times [0, t_{max}] \\ & \quad (23) \end{aligned}$$

$$\begin{aligned} \frac{\partial \Psi}{\partial n} - (\mathbf{v}_f \cdot \mathbf{n})\Psi &= \theta, \quad (\mathbf{x}, t) \in \Gamma_I \times [0, t_{max}] \\ & \quad (24) \end{aligned}$$

The steps for the derivation of such *adjoint problems* are given in reference [7], where inverse convection problem in fixed enclosures was considered.

We are further looking at the *sensitivity problem*. The sensitivity temperature field $\Theta(\mathbf{x}, t; q_{ol}, \Delta q_{ol}) \equiv D_{\Delta q_{ol}} \theta(\mathbf{x}, t; q_{ol})$, and the sensitivity velocity field $\mathbf{U}(\mathbf{x}, t; q_{ol}, \Delta q_{ol}) \equiv D_{\Delta q_{ol}} \mathbf{u}(\mathbf{x}, t; q_{ol})$ are defined as the

linear Δq_{ol} parts of $\theta(\mathbf{x}, t; q_{ol} + \Delta q_{ol})$ and $\mathbf{u}(\mathbf{x}, t; q_{ol} + \Delta q_{ol})$ calculated at q_{ol} , i.e.

$$\begin{aligned} \theta(\mathbf{x}, t; q_{ol} + \Delta q_{ol}) &= \theta(\mathbf{x}, t; q_{ol}) + \Theta(\mathbf{x}, t; q_{ol}, \Delta q_{ol}) \\ &+ O(\|\Delta q_{ol}\|_{L_2(\Gamma_o \times [0, t_{max}])}^2) \end{aligned} \quad (25)$$

$$\begin{aligned} \mathbf{u}(\mathbf{x}, t; q_{ol} + \Delta q_{ol}) &= \mathbf{u}(\mathbf{x}, t; q_{ol}) + \mathbf{U}(\mathbf{x}, t; q_{ol}, \Delta q_{ol}) \\ &+ O(\|\Delta q_{ol}\|_{L_2(\Gamma_o \times [0, t_{max}])}^2) \end{aligned} \quad (26)$$

The governing equations for the *sensitivity problem* are:

$$\frac{\partial \Theta}{\partial t} + \mathbf{u} \cdot \nabla \Theta + \mathbf{U} \cdot \nabla \theta = \nabla \cdot \nabla \Theta \quad (27)$$

$$\begin{aligned} \frac{\partial \mathbf{U}}{\partial t} + \mathbf{u} \cdot \nabla \mathbf{U} + \mathbf{U} \cdot \nabla \mathbf{u} &= \nabla \cdot \Sigma - PrRa\Theta \mathbf{e}_g \\ & \quad (28) \end{aligned}$$

$$\Sigma = -\Pi \mathbf{I} + Pr [\nabla \mathbf{U} + (\nabla \mathbf{U}^T)] \quad (29)$$

$$\nabla \cdot \mathbf{U} = 0 \quad (30)$$

$$\Theta(\mathbf{x}, 0) = 0, \quad \mathbf{x} \in \Omega \quad (31)$$

$$\mathbf{U}(\mathbf{x}, 0) = 0, \quad \mathbf{x} \in \Omega \quad (32)$$

$$\mathbf{U}(\mathbf{x}, t) = 0, \quad (\mathbf{x}, t) \in \Gamma \times [0, t_{max}] \quad (33)$$

$$\Theta(\mathbf{x}, t) = 0, \quad (\mathbf{x}, t) \in \Gamma_g \times [0, t_{max}] \quad (34)$$

$$\begin{aligned} \frac{\partial \Theta}{\partial n}(\mathbf{x}, t) &= 0, \quad (\mathbf{x}, t) \in (\Gamma_h + \Gamma_I) \times [0, t_{max}] \\ & \quad (35) \end{aligned}$$

$$\begin{aligned} \frac{\partial \Theta}{\partial n}(\mathbf{x}, t) &= \Delta q_{ol}(\mathbf{x}, t), \quad (\mathbf{x}, t) \in \Gamma_o \times [0, t_{max}] \\ & \quad (36) \end{aligned}$$

We have outlined the formulation for *direct*, *adjoint* and *sensitivity problems*. The conjugate gradient method (CGM) is used for the minimization of the cost functional $S(q_{ol})$. It constructs a sequence: $q_{ol}^0, q_{ol}^1, \dots, q_{ol}^k, \dots$, to approach the optimal minimizer q_{ol} . The procedure is as follows:

Step A: Make an initial guess of $q_{ol}^0(\mathbf{x}, t) \in L_2(\Gamma_o \times [0, t_{max}])$ and set $k = 0$

Step B: Calculate the conjugate search direction $p^k(\mathbf{x}, t), (\mathbf{x}, t) \in \Gamma_o \times [0, t_{max}]$

1. Solve the direct problem for $\theta(\mathbf{x}, t; q_{ol}^k)$ and $\mathbf{u}(\mathbf{x}, t; q_{ol}^k)$

2. Compute the residual $\theta(\mathbf{x}, t; q_{ol}^k)$ for $(\mathbf{x}, t) \in \Gamma_I \times [0, t_{max}]$

3. Solve the adjoint problem backward in time for $\Psi(\mathbf{x}, t; q_{ol}^k)$

4. Set $S'(q_{ol}^k) = \Psi(\mathbf{x}, t; q_{ol}^k), (\mathbf{x}, t) \in \Gamma_o \times [0, t_{max}]$

5. Set $\gamma^k = 0$, if $k = 0$; otherwise: $\gamma^k = \frac{(S'(q_{ol}^k), S'(q_{ol}^k) - S'(q_{ol}^{k-1}))_{L_2(\Gamma_o \times [0, t_{max}])}}{\|S'(q_{ol}^{k-1})\|_{L_2(\Gamma_o \times [0, t_{max}])}^2}$

6. Define $p^k(\mathbf{x}, t)$, If $k = 0$, $p^0 = -S'(q_{ol}^0)$; Otherwise, $p^k = -S'(q_{ol}^k)(\mathbf{x}, t) + \gamma^k p^{k-1}$

Step C: Calculate the optimal step size α^k

1. Solve the sensitivity problem for $\Theta(\mathbf{x}, t; q_{ol}^k, p^k)$ and $\mathbf{U}(\mathbf{x}, t; q_{ol}^k, p^k)$
2. Calculate α^k by $\alpha^k = \frac{-(S'(q_{ol}^k), p^k)_{L_2(\Gamma_o \times [0, t_{max}])}}{\|\Theta(\mathbf{x}, t; q_{ol}^k, p^k)\|_{L_2(\Gamma_I \times [0, t_{max}])}^2}$

Step D: Update $q_{ol}^{k+1}(\mathbf{x}, t) = q_{ol}^k(\mathbf{x}, t) + \alpha^k p^k(\mathbf{x}, t)$, $(\mathbf{x}, t) \in \Gamma_o \times [0, t_{max}]$

Step E: If $\|q_{ol}^{k+1} - q_{ol}^k\|_{L_2(\Gamma_o \times [0, t_{max}])} < \epsilon$ (specified tolerance), stop; Otherwise, set $k = k + 1$ and go to Step B.

The inner product in L_2 space involved in CGM procedure is defined as:

$$(f, g)_{L_2(\Gamma \times [0, t_{max}])} = \int_0^{t_{max}} \int_{\Gamma} f g d\Gamma dt \quad (37)$$

NUMERICAL EXAMPLE AND IMPLEMENTATION

We are looking at the following two-dimensional solidification problem. Liquid melt at uniform initial temperature $\theta_i (\theta_i > 0)$, is confined in a rectangular closure ($0 \leq x \leq 0.5$, $0 \leq y \leq 1$) bounded by a mold. The top and bottom walls are always kept adiabatic. The solidification is driven by the cooling heat flux q_{os} at the solid mold boundary $x = 0$. The schematic configuration is shown in Figure 2. The non dimensional parameters for liquid are $Pr = 0.0149$, $Ra = 10^4$ and the Stefan number (ratio of initial superheating sensible heat to solidification latent heat) $Ste = \frac{c_l(T_i - T_m)}{L} = 0.25$.

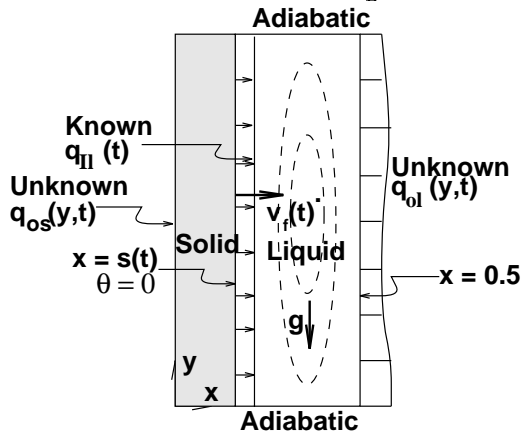


FIGURE 2: Schematic of the example problem.

We are interested to design the solidification process such that a flat (vertical) freezing front is obtained moving with a desired growth velocity $v_f(t)$ and with a desired heat flux $q_{II}(t)$. Note that both $v_f(t)$ and $q_{II}(t)$

are independent of y . In such a process and at each time t , a uniform microstructure will be obtained along the y direction. In order for such a sharp flat interface to advance stably (without developing any dendritic or mushy morphology), we restrict the heat flux q_{II} at the interface liquid side and the growth velocity v_f by the following relation:

$$\left| \frac{q_{II}}{v_f} \right| \geq 1 \quad (38)$$

This is just the non-dimensional form of equation (1). The concentration level C_o is chosen to be small enough such that

$$\frac{|m_l|(1-k)C_o}{T_i - T_m} \leq \frac{D_l}{\alpha} \quad (39)$$

We choose $q_{II}(t)$ based on an adjustment of $\hat{q}_{II}(y, t)$, which is the interface heat flux when the liquid mold wall is adiabatic and $v_f(t) = 5$. Such a $\hat{q}_{II}(y, t)$ is obtained from a FEM solution of a direct natural convection problem in the liquid region, with boundary conditions $\theta(5t, y; t) = \theta_m = 0$ at the freezing interface and $q_{ol}(y, t) = 0$ ($0 \leq y \leq 1$) at $x = 0.5$. For the solution of this direct problem, we used a 20×20 uniform bilinear quadrilateral element mesh and a time step of $\Delta t = 2 \times 10^{-4}$. Then the specific choices for $v_f(t)$ and $q_{II}(t)$ for the inverse design problem are:

$$v_f(t) = \begin{cases} 5, & 0 \leq t < t_{mid} \\ 5 \frac{(t_{max} - t)}{(t_{max} - t_{mid})}, & t_{mid} \leq t \leq t_{max} \end{cases} \quad (40)$$

and

$$q_{II}(t) = \begin{cases} \int_0^1 \hat{q}_{II}(y, t) dy, & 0 \leq t < t_{mid} \\ -5 \frac{(t_{max} - t)}{(t_{max} - t_{mid})}, & t_{mid} \leq t \leq t_{max} \end{cases} \quad (41)$$

where $t_{max} = 0.13$ and t_{mid} is defined from $\int_0^1 \hat{q}_{II}(y, t_{mid}) dy = -5$. From our computations, it turns out that $t_{mid} = 0.052$. In other words, we are taking y-average of $\hat{q}_{II}(y, t)$ as $q_{II}(t)$ under constant $v_f(t)$ before t_{mid} , and afterwards a linearly decreasing profile for $v_f(t)$ and $q_{II}(t)$, down to 0, when $t = t_{max}$.

It is usual to have q_{II} approaching zero near the completion of solidification when advection will eliminate any superheating in the liquid region as the size of the melt approaches zero. A slowing down growth velocity v_f is chosen accordingly to satisfy equation (38). $q_{II}(t)$ is shown in Figure 3, where for comparison $\int_0^1 \hat{q}_{II}(y, t) dy$ is also given as the lower line.

The heat flux at the interface solid side $q_{Is}(t)$ can be calculated from the Stefan condition as follows:

$$q_{Is}(t) - q_{II}(t) = Ste^{-1} v_f(t) \cdot n \quad (42)$$

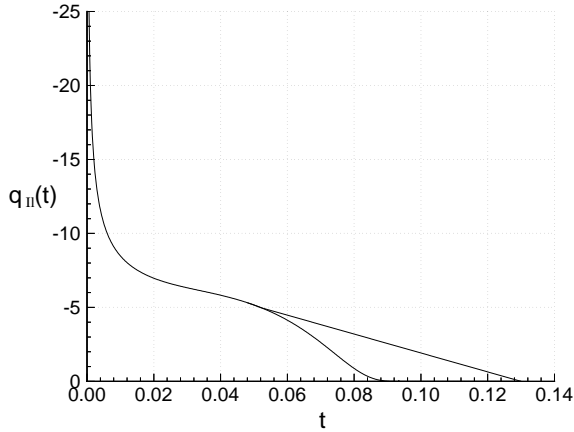


FIGURE 3: Interfacial heat flux (liquid side) $q_{II}(t)$

where n is defined as in Figure 1. The calculation of q_{os} and q_{ol} can be performed by solving two uncoupled inverse problems; an inverse conduction problem in the solid region and an inverse convection problem in the melt. Here, the inverse conduction problem is one-dimensional, while a two-dimensional inverse convection problem must be addressed.

The inverse problem in the solid region is to find the boundary heat flux $q_{os}(t)$ at $x = 0$ that results in a freezing interface moving at velocity $v_f(t)$ with heat flux $q_{Is}(t)$. There is only heat conduction in the solid, and the inverse formulation and solution procedure can be found in [3-6]. The problem is reduced to one spatial dimension (no variation in the y direction). We use 20 uniformly spaced moving linear elements (in the x -direction) and the time step was taken as $\Delta t = 2 \times 10^{-4}$.

The inverse problem in the liquid is to compute $q_{ol}(y, t)$ at $x = 0.5$ of the mold wall in order to obtain the desired interface velocity $v_f(t)$ and heat flux $q_{II}(t)$ on the liquid side of the front. 20×20 uniform quadrilateral elements are used with bilinear shape functions for both temperature and velocity. The penalty number for enforcement of the incompressibility condition is 10^8 . A moving finite element approach is taken to handle the shrinking of the liquid region. A streamlined upwind Petrov-Galerkin scheme is used for the direct, adjoint and sensitivity equations. Details of the matrix formulation and time integration for the direct, adjoint and sensitivity problems are following reference [11], while more specific details can be found in [7]. The time step is $\Delta t = 2 \times 10^{-4}$. The time stepping is carried out up to total of 650 steps until the solidification interface reaches $s(t_{max}) = 0.45$, where 90% of the original liquid has solidified. The inverse calculation is computationally intensive and each global iteration with solutions of direct, adjoint and sensitivity prob-

lems needs approximately 84 minutes CPU time on a DEC alpha-station 200.

RESULTS AND DISCUSSION

Figure 4 shows the optimal heat flux history $q_{os}(t)$ at the vertical solid mold wall. The initial large heat flux results from the sudden start of solidification at $t = 0^+$. Afterwards, two competing factors are influencing the trend of $q_{os}(t)$. The constant velocity v_f before t_{mid} requires an increasing heat flux input at $x = 0$, because of a constantly growing solid region; the decreasing $q_{II}(t)$ needs less cooling from $q_{os}(t)$. After the initial transient, such factors balance each other at $t \sim 0.035$, where a peak of $q_{os}(t)$ occurs. After this time, q_{os} is decreasing.

For the inverse problem in the liquid, the optimal temporal and spatial variations of the heat flux $q_{ol}(y, t)$ at the liquid mold wall are shown in Figure 5. Figure 6 plots $q_{ol}(y, t)$'s spatial variation at different fixed time levels. Figure 7 shows the objective function's minimization process with the iterations of the conjugate gradient method. The CGM iterations start with a initial guess $q_{ol}(y, t) = 0$ and go up to 100 iterations when $\|q_{ol}^{k+1} - q_{ol}^k\| < 10^{-4}$.

The temperature and flow fields in the liquid corresponding to this optimal heat flux are displayed in Figure 8 at different stages of solidification. The blank region at the left part of the mold is the solidified part. Part (a) of Figure 8 draws 10 levels of isotherms in the liquid region that are equally spaced in terms of temperature value. The lowest level $\theta = 0$ is at the solid-liquid interface $x = s(t)$ and the highest level is the most right curve that has its value indicated as θ_{max} on the top of each figure. Part (b) of Figure 8 displays the contours of the stream function ψ , which are computed from the velocity field via the Galerkin finite element solution of $\nabla^2 \psi = -\nabla \times \mathbf{u}$. For each (b), there are 8 levels of contours with equal spaced ψ values. The $\psi_{max} = 0$ contour is taken as the boundary of the liquid melt: $x = s(t)$, 0.5 and $y = 0, 1$. As we can see, there is only one major convection flow cell (anti-clockwise) in the liquid melt. The magnitude of the y -component velocity $|\frac{\partial \psi}{\partial x}|$ is largest near the moving interface.

The spatial variation of $q_{ol}(y, t)$ is only significant before $t \sim 0.06$. It can be seen from Figures 8(1a), 8(2a) and 8(3a), that the isotherms near the right liquid mold wall are touching the wall or are distorted, while in Figure 8(4a), all the isotherms are almost vertical straight lines. The boundary heat flux distribution in the y -direction at the liquid mold wall adjusts the thermal and flow fields in such a way that a vertical isotherm $\theta = 0$ results at the solid-liquid interface $x = s(t)$ according to our inverse design objective. This flux variation matches the temporal characteristics of convection observed in Figures 8(b). In these figures, one can first

see a growing strength of convection flow, then a maximum flow strength sometime between $t = 0.02$ and $t = 0.05$, and eventually a diminishing flow.

The temporal variation of $q_{ol}(y, t)$ is first an increasing trend of heating up to $t \sim 0.08$, when a maximum is reached, then a gradual decrease down to zero (Fig. 6). This can be explained by the fact that after t_{mid} , $q_{II}(t)$ at the moving interface is stronger than $\int_0^1 \hat{q}_{II}(y, t) dy$, as shown in Figure 3. Thus, heat input is needed at the liquid mold wall to balance a higher $q_{II}(t)$. The overall heating at $x = 0.5$ starts earlier than $t_{mid} = 0.52$, which allows the heat transfer across the liquid region to influence the liquid temperature gradient adjacent to the moving interface. On the other hand, the interface velocity is slowed down after t_{mid} . Compared to the constant v_f case, a wider domain of liquid is left for a given time and less heating is needed at $x = 0.5$. These two factors lead to the appearance of maximum heating on the liquid mold wall at $t \sim 0.08$. Finally, when $q_{II}(t)$ tends to zero and the temperature field in the liquid is nearly uniform, $q_{ol}(y, t)$ also reduces its value towards zero.

CONCLUSIONS

An inverse solidification design problem with natural convection is solved with the adjoint method and a functional optimization scheme. Both the growth velocity and the heat flux at the solid-liquid interface are controlled through the thermal boundary conditions at the mold wall. This enables the control of microstructural development during solidification. The designed growth velocity and interface heat flux can be chosen to satisfy the stability criteria for planar interface, thus avoiding dendritic or mushy morphology. It is of future interest to introduce the concentration field for alloys for such inverse solidification design problems. This will make the stability consideration more rigorous by including both melt convection and solute diffusion. Solidification process control can also be realized by distributed heat sources or positive forced convection such as electro-magnetic stirring. The design and modeling of solidification processes for such cases is extremely challenging and of practical importance.

ACKNOWLEDGEMENT

The results presented in this paper were obtained in the course of research sponsored by the National Science Foundation under grant CTS-9115438 to Cornell University and with support from Alcoa Laboratories. The computing for this project was supported by the Cornell Theory Center. The authors gratefully acknowledge these contributions.

REFERENCES

- [1] W. Kurz and D. J. Fisher, *Fundamentals of Solidification*, (Trans Tech Publications Ltd, Switzerland, 1989).
- [2] M. C. Flemings, *Solidification Processing*, McGraw-Hill, New York, 1974.
- [3] N. Zabarar, Y. Ruan and O. Richmond, On the design of two-dimensional Stefan processes with desired freezing front motions, *Numerical Heat Transfer*, 21B (1992) 307-325.
- [4] N. Zabarar and S. Kang, On the solution of an ill-posed inverse solidification problem using minimization techniques in finite and infinite dimensional function spaces, *Int. J. Num. Meth. Eng.*, 36 (1993) 3973-3990.
- [5] S. Kang and N. Zabarar, Control of the freezing interface motion in two-dimensional solidification processes using the adjoint method, *Int. J. Numer. Methods. Engr.*, 38 (1995) 63-80.
- [6] N. Zabarar and T. Hung Nguyen, Control of the freezing interface morphology in solidification processes in the presence of natural convection, *Int. J. Num. Meth. Eng.*, 38 (1995) 1555-1578.
- [7] N. Zabarar and G. Yang, A functional optimization formulation and implementation of an inverse natural convection problem, submitted to *Comp. Methods Appl. Mech. Engr.*
- [8] J. V. Beck, B. Blackwell and C. R. St. Clair, Jr., *Inverse Heat Conduction, Ill-posed Problems*, (Wiley-Interscience, New York, 1985).
- [9] W. W. Mullins and R. F. Sekerka, Stability of a planar interface during solidification of a dilute alloy, *Journal of Appl. Phys.*, 35 (1964), 444-451.
- [10] J. W. Rutter and B. Chalmers, Prismatic substructure, *Can. J. Phys.*, 31 (1953), 15-39.
- [11] A. N. Brooks and T. J. R. Hughes, Streamline upwind/Petrov-Galerkin formulations for convection dominated flows with particular emphasis on the incompressible Navier-Stokes equations, *Comp. Methods Appl. Mech. Engr.*, 32 (1982) 199-259.

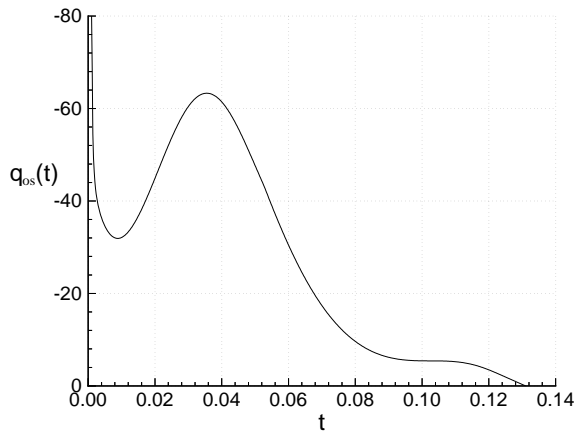


FIGURE 4: Optimal heat flux $q_{os}(y, t)$ at the solid mold wall.

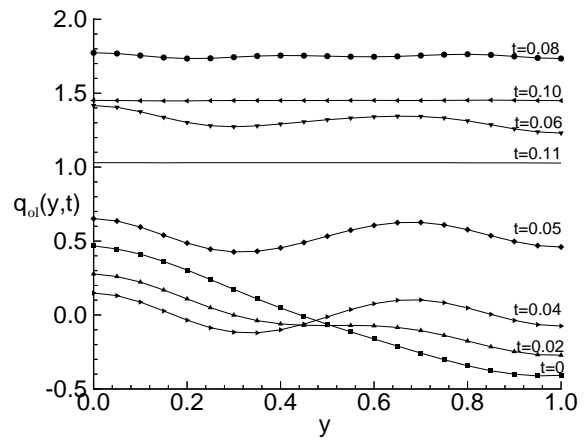


FIGURE 6: $q_{oi}(y, t)$ distribution at different time levels.

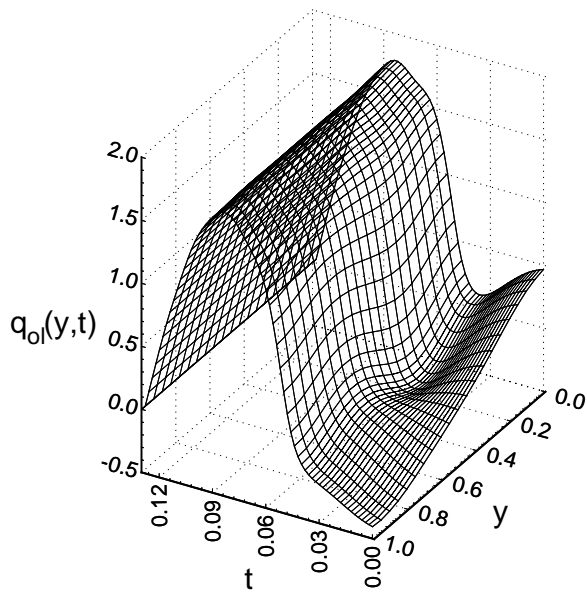


FIGURE 5: Optimal heat flux $q_{oi}(y, t)$ at the liquid mold wall.

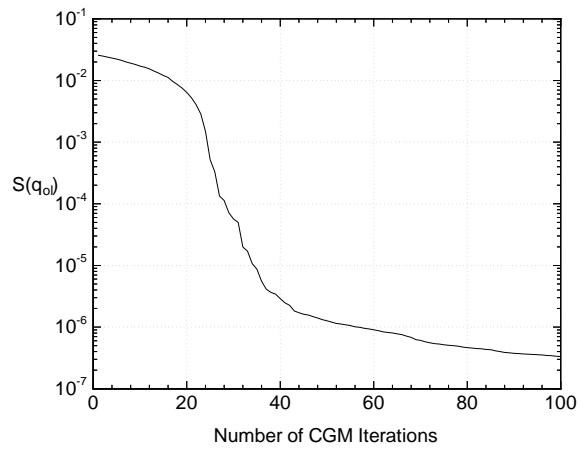


FIGURE 7: Objective function's minimization with CGM Iterations.

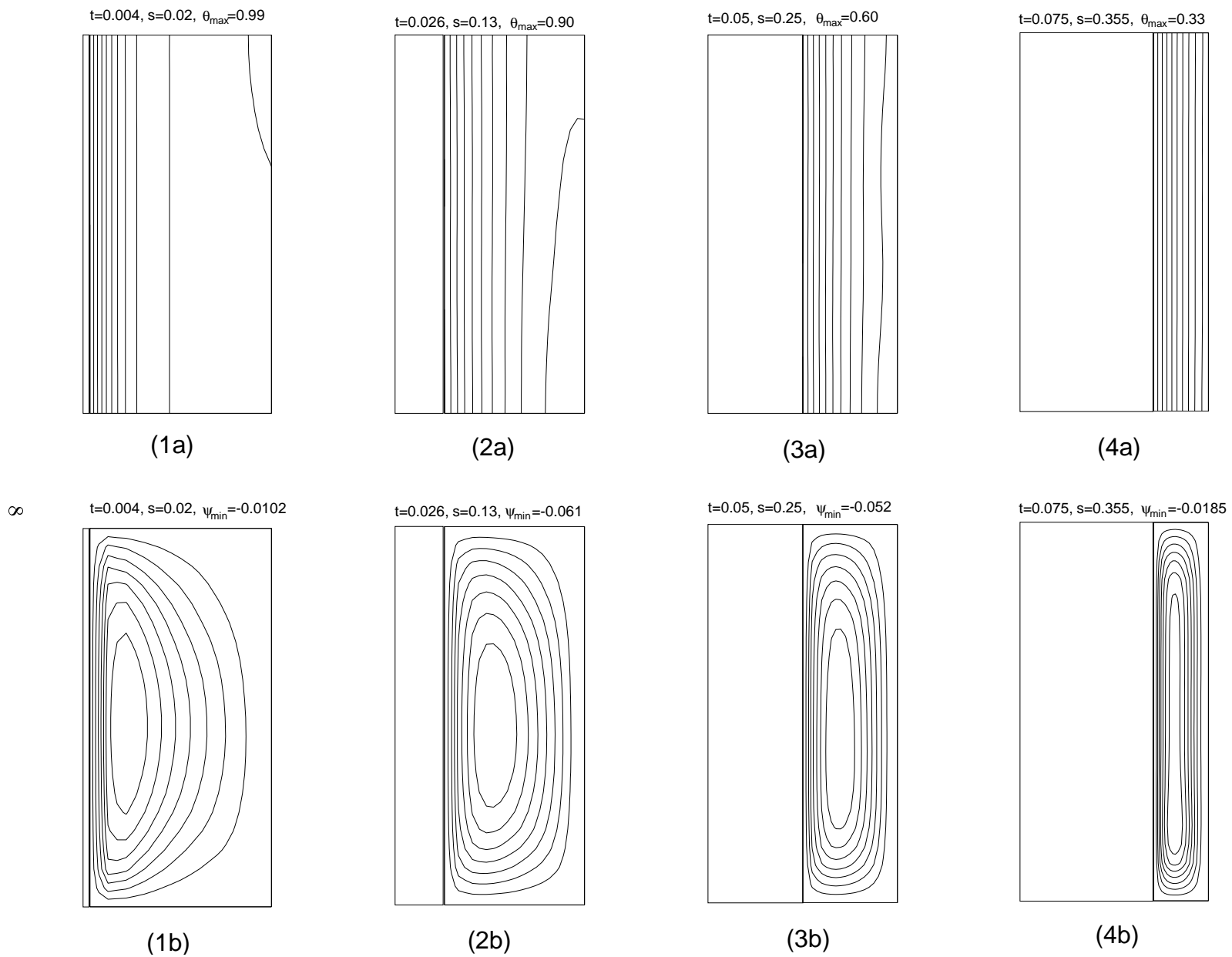


FIGURE 8: Temperature and flow field